Appl. Phys. A (2015) 118:1189–1196
DOI 10.1007/s00339-014-8868-3

Applied Physics A
Materials Science & Processing

Femtosecond laser color marking stainless steel surface with different wavelengths

Guoqiang Li · Jiawen Li · Yanlei Hu · Chenchu Zhang · Xiaohong Li · Jiaru Chu · Wenhao Huang

Received: 18 July 2014 / Accepted: 31 October 2014 / Published online: 9 November 2014

Abstract The femtosecond laser color marking stainless steel surfaces with different incident wavelengths were investigated theoretically and experimentally. It indicates that the spectral regions of the colors firstly increase and then reduce with increasing spatial periods of the ripples induced by laser irradiation. Additionally, the colors are gradually changed from blue to red due to the elongation of the diffracted light wavelengths. As a result, the color effects are distinctly different. This study offers a new controllable parameter to produce diverse colors, which may find a wide range of applications in the laser color marking, art designing and so on.

1 Introduction

Femtosecond laser-induced periodic surface structures (LIPSSs) on metals surfaces, frequently simply called "ripples," have been extensively investigated for diverse applications [1–9]. Recently, it is found that the sub-wavelength ripples have a distinct feature of acting as surface grating which can powerfully alter the optical property on the metal surfaces [10–15]. The pioneering work indicated that colorizing metals by femtosecond laser-induced periodic ripples can be realized with suitable laser fluence level and scanning speed [10–14]. It is reported that the formed ripples directions are always depending on laser polarization [16]. This directional dependence can be utilized to mark the surfaces with different oriented ripples to form different colors which are sensitive to incident light coming from a certain direction [10–15]. In addition to this, we recently have reported the control of the color effects on aluminum surfaces just by adjusting the pulse overlaps [15]. From the above, the colors on metal surfaces can be controlled by optimizing the laser processing parameters, such as the laser fluence, scanning speed and laser polarization and so on.

We find that the ripple's period is directly dependent on the laser wavelength and the materials [17]. To the best of our knowledge, most papers indicate that the colors are produced with laser wavelength of about 800 nm, and the corresponding ripples periods ranged from 480 to 580 nm. However, the structural colors formed by other laser wavelength are less researched. In this paper, a systematic study is performed on the dependence of structural colors on the laser wavelengths which ranged from 400 to 2,200 nm. It is found that completely different colors can be obtained by different types of ripples induced with varying laser wavelengths. The discussion in this paper suggests femtosecond laser wavelength as a potential parameter to fabricate various colors and ultimately leads to controlling the optical properties of the metals.

2 Experimental

The experiments were conducted to study the colors which are formed by a variety of subwavelength ripples induced

G. Li · J. Li (✉) · Y. Hu (✉) · C. Zhang · J. Chu · W. Huang
Department of Precision Machinery and Precision Instrumentation, University of Science and Technology of China, Hefei 230026, China
e-mail: jwl@ustc.edu.cn

Y. Hu
e-mail: huyl@ustc.edu.cn

G. Li
e-mail: guoqli@mail.ustc.edu.cn

X. Li
School of Science, Southwest University of Science and Technology, Mianyang 621010, China

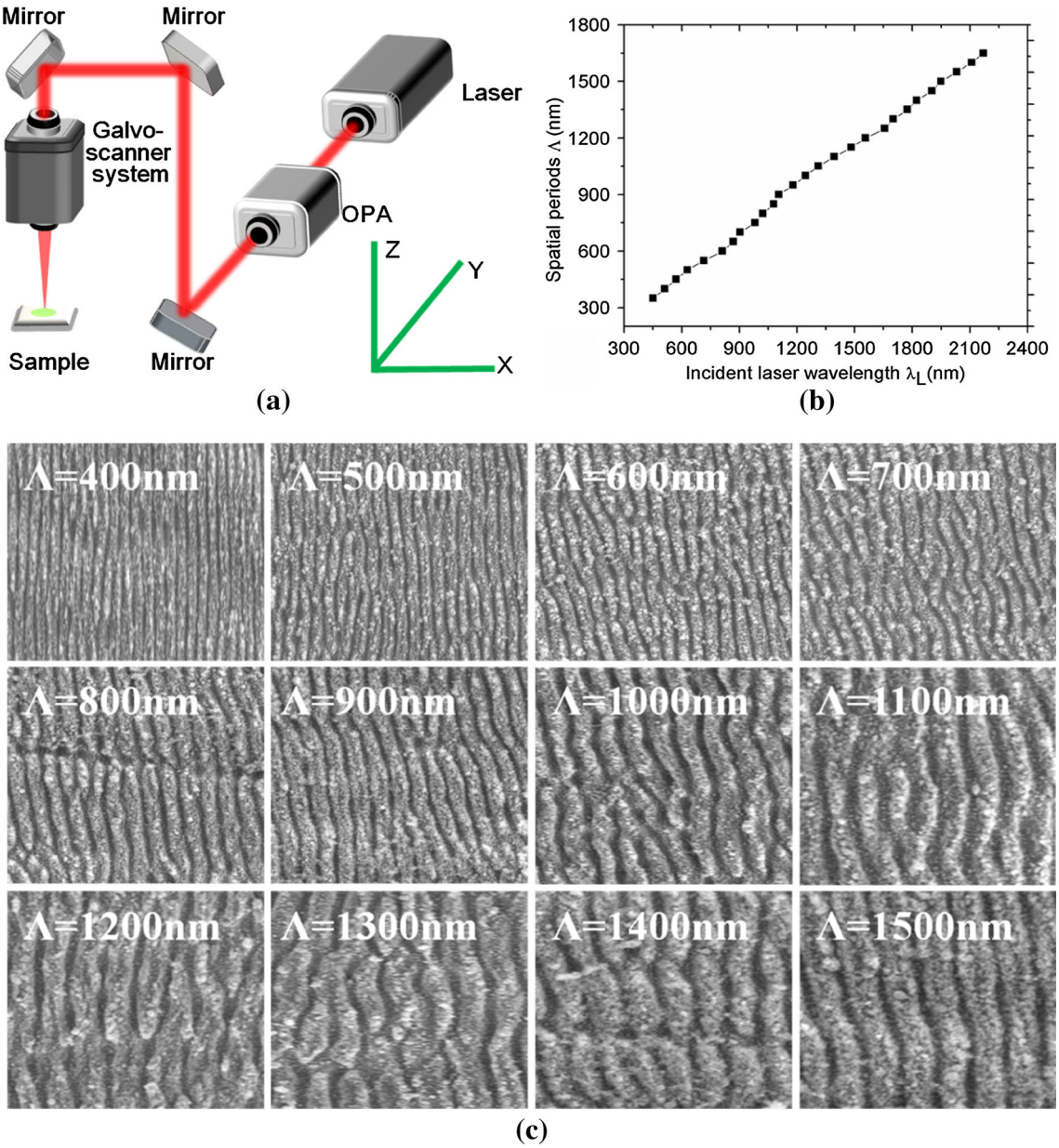

Fig. 1 **a** Schematic diagram of the experimental set up. **b** Ripple spatial periods as a function of the incident laser wavelength. **c** Partial SEM images for the laser-induced periodic surface structures by different laser wavelengths

with varying laser wavelengths. For this purpose, an amplified Ti: sapphire femtosecond laser system that consists of a mode-locked oscillator (Chameleon VISION-S) and a regenerative amplifier (Legend Elite-1 K-HE) was applied to scan the mirror polished 316L stainless steel surface. The schematic diagram of the experimental setup is shown in Fig. 1a. The laser system generates pulses with the width of 104 fs at repetition rate of 1 kHz. The laser wavelength, a key processing parameter, is modulated by the optical parametric amplifier (OPA, TOPAS-800-fs), and the modulation range is from 240 to 2,600 nm. The laser beam is horizontally polarized and is focused vertically onto the samples by an x–y galvo with a flat field lens. The beam diameter focused at the sample surface is about 20 μm. Before laser surface treatment, the laser power was adjusted via a linear Glan–Taylor polarizer combining a half-wave plate. The surface morphology of structural modifications on the stainless steel samples was examined with a scanning electron microscope (SEM).

It indicates that ripples with various kinds of periods can be induced by different laser wavelength under suitable laser fluence and scanning speed. The exact calculation for spatial period Λ is still difficult [18–20]. However, the goal of our work was to obtain the needed ripple periods by

precisely controlling the laser wavelengths experimentally. It is found that uniform ripples with different spatial periods can be obtained at optimized laser fluence in the range of 0.96–1.02 J/cm^2, scanning speed of 13 mm/s. The ripple spatial periods (Λ) as a function of the incident laser wavelength (λ_L) are illustrated in Fig. 1b. The partial SEM images of the ripples formed on stainless steel surface are presented in Fig. 1c.

3 Results and discussion

The results in Fig. 1b and c show that the spatial periods of LIPSS depend on the laser fluence and the incident laser wavelength. The formation mechanism has been studied by Sakabe et al. [18] and Okamuro et al. [19]. The ripple spatial periods (Λ) can be expressed as

$$\Lambda = \lambda_L \left\{ 1 + \left(\frac{n_{es} \cdot e^2 \cdot \lambda_L^2}{mc^2} - 2 \right)^{-1} \right\}^{-1/2} \quad (1)$$

where λ_L is the incident laser wavelength, n_{es} is the surface electron density induced by the incident laser, c is the speed of light in vacuum, e is the electron charge, and m is the electron mass, respectively. n_{es} in our case is influenced by the laser fluence and the incident laser wavelength. From Eq. 1, an obvious and direct correspondence can be obtained between ripple spatial periods Λ and incident laser wavelength λ_L. To study the formed colors, we regard the ripples as gratings [21–24]. It is known that the diffracted light by the ripples strongly depend on the light source directions and the ripple directions. Therefore, the sample is examined under the color measuring system, as shown in Fig. 1d. It indicates that the horizontally mounted sample, rotated around Z-direction, is illuminated by an unpolarized light source which is placed in the XZ plane, with α orientation to the Z-direction, equivalent to the day–light spectrum. φ is the ripple direction to X-direction. Both the ranges of α and φ are from 0° to 90°. Then, the diffracted light is observed with a β orientation to the Z-direction, at the contrary direction of light source. In our study, the viewing angle is fixed at 20°.

The gratings with different spatial periods having a size of 5 mm × 5 mm are examined under the color measuring system as shown in Fig. 2a. The photographs are taken by means of a conventional digital camera (Canon, IXUS 95 IS). The results are shown in Fig. 3. It is indicated that the colors are different at different coordinates for a given ripple period. In addition, the observed colors are also different at the same coordinates for different ripple periods.

Based on the color measuring system, a related theoretical simulation can be performed through the analysis of the diffraction equations with different periods. The diffraction equation [24]can be written as:

$$n\lambda = \Lambda(\sin\alpha \cdot \sin\varphi + \sin\beta) \quad (2)$$

where λ is the wavelength of white light, and the range is from 400 to 700 nm, covering the whole visible spectrum. n is the order of diffraction. The schematic diagram of the diffraction of light at the grating is shown in Fig. 2b. The wavelength of second-order diffraction light is <400 nm which cannot be observed for most spatial periods. In addition, the intensity of the second-order diffraction light or even higher orders is so weak that it can be ignored. Hence, only the first-order diffraction from the grating can be selected, namely $n = 1$. From the calculated spatial periods matching the different diffracted wavelengths, it is observed that the processed areas can exhibit structural colors when the period Λ is >298 nm and <2,047 nm. When the ripples period is beyond this scope, there is no wavelength λ found to fulfill the diffraction conditions, thus no color can be observed. In addition, the colors can cover the whole visible spectrum if the spatial period is >522 nm and <1,170 nm. As described above, we can divide the periods into three scopes, namely 298 to 522 nm, 522 to 1,170 nm and 1,170 to 2,047 nm, to separately study the influence of periods on the color effects.

Firstly, the spatial periods ranged from 298 to 522 nm is discussed. By solving the diffraction equation, α and φ matching different periods are calculated. Then, the calculated α and φ are set to horizontal and vertical coordinates, respectively. The segmental results are presented in Fig. 4. One can see that the silhouette which is besieged by α and φ meeting the diffraction equation (marked blue in figures, hereinafter referred to as "silhouette") present a completely symmetric about the angular bisector of the coordinate system.

By comparison, obviously, at low spatial period of 300 nm, the diffracted light can cover only a few nanometers, namely from $\lambda = 400$ to 403 nm, as shown in Fig. 4a. As the periods increase, a broader spectrum appears and the maximum value of the spectrum increases (Fig. 4b, c). When the periods are increased to 521.6 nm, the whole visible spectrum can be covered (Fig. 4c). Moreover, the locations of the silhouettes are getting closer to coordinate axes.

In order to get a deep insight into the influence of the spatial periods on the transfer of the spectrum, we calculate the locations of spectrum $\lambda = 400$, 500, 600 and 700 nm in the α, φ coordinate system, which are presented in Fig. 4d–f. For $\Lambda = 300$ nm, it indicates that only the spectrum of $\lambda = 400$ nm can be observed near (90°, 90°), presenting an arc-shaped line, which is symmetric about the angular bisector of the coordinate system. When Λ is increased to

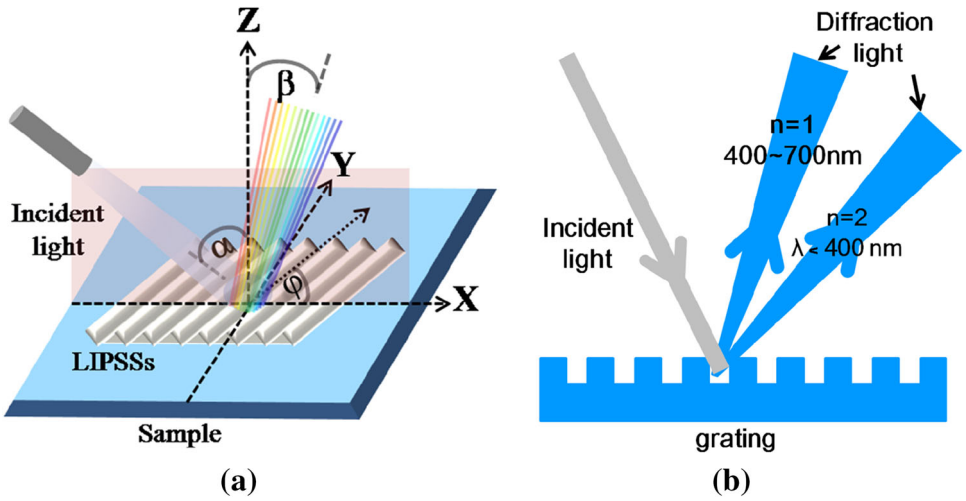

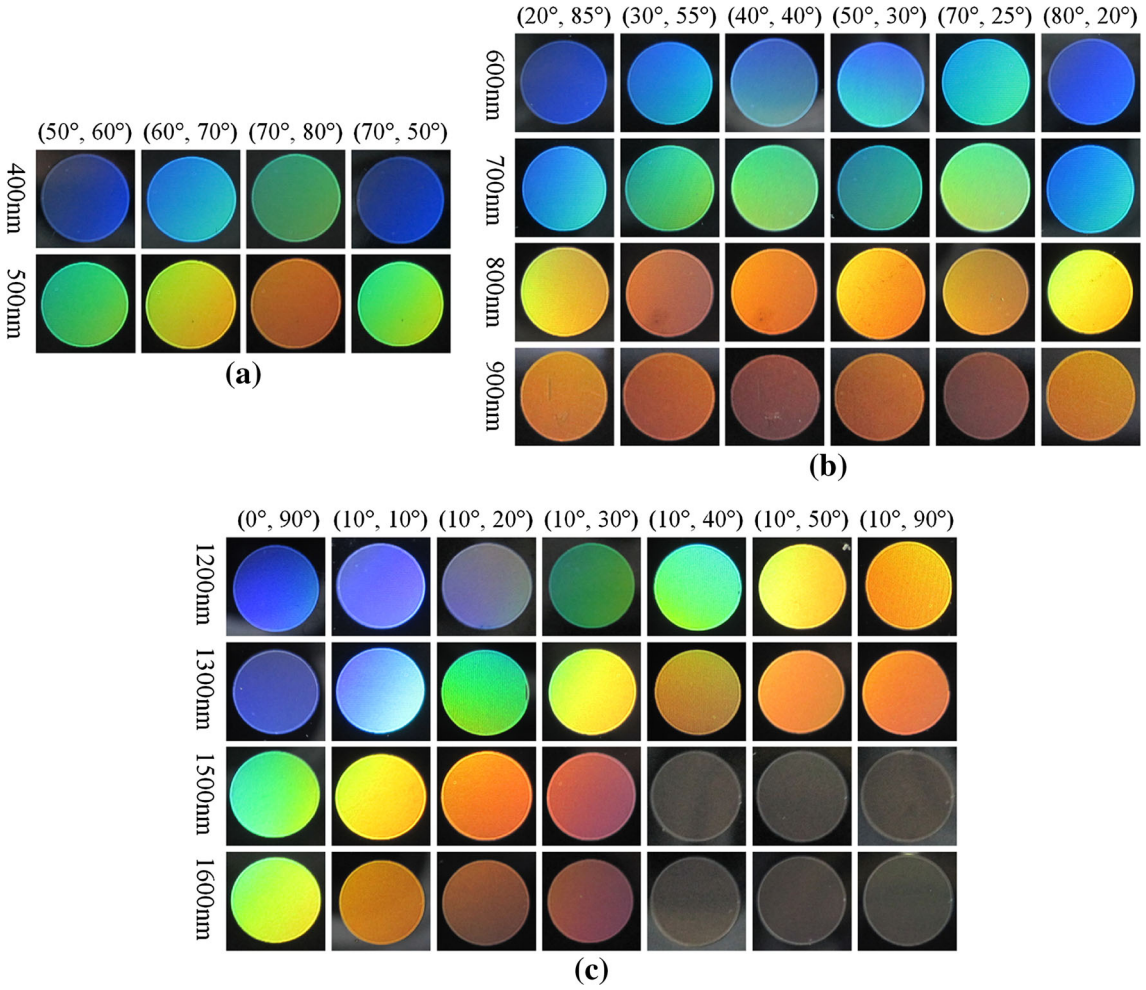

Fig. 2 **a** Color measuring system. **b** Schematic diagram of the diffraction of light at the grating

Fig. 3 Photographs of the structural colors formed with different spatial periods

400 nm, the coordinate areas for the spectrum $\lambda = 400$ nm becomes broader. In addition, the spectrum $\lambda = 500$ nm appears. However, it is noticed that the two spectra are away from each other, which is demonstrated in Fig. 4e. As Λ becomes 521.6 nm, it is the lower limit of the Λ meeting the condition to cover the whole visible spectrum. In this

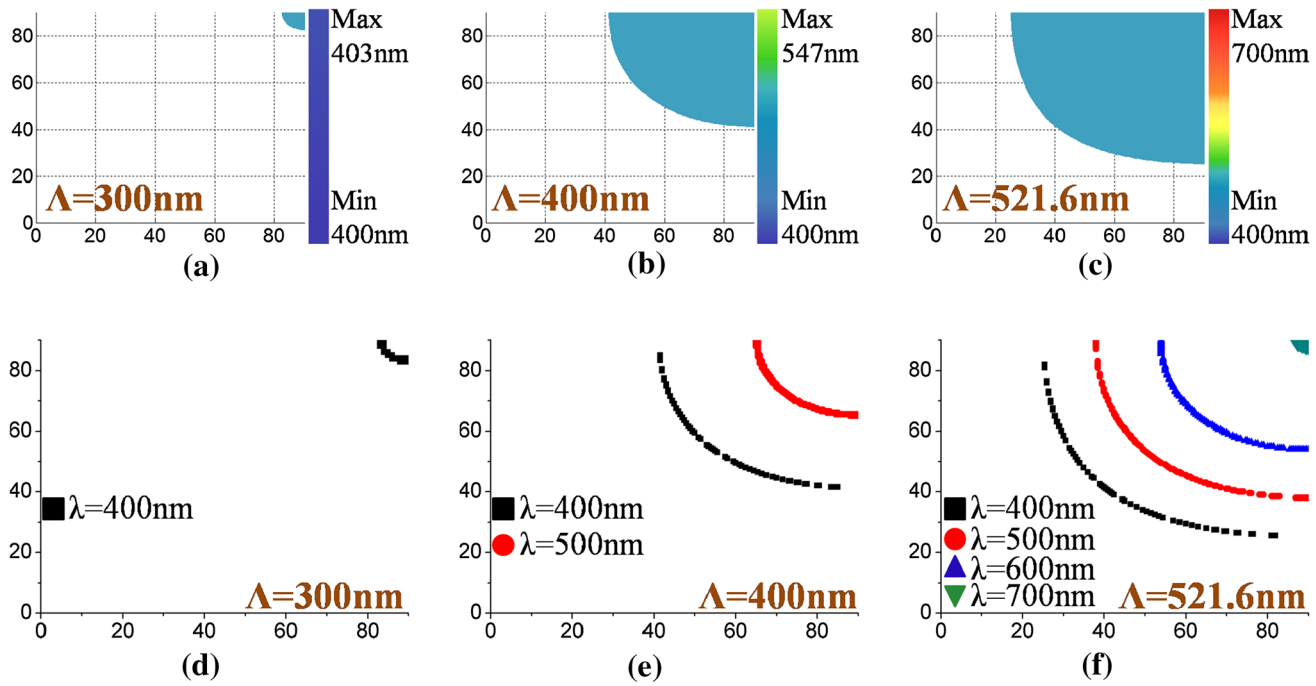

Fig. 4 Calculated coordinate meeting the diffraction equation and spectrum for the structural colors formed under the spatial periods of 298 and 522 nm. The *bars* on the right of **a**, **b** and **c** indicate the spectrum range

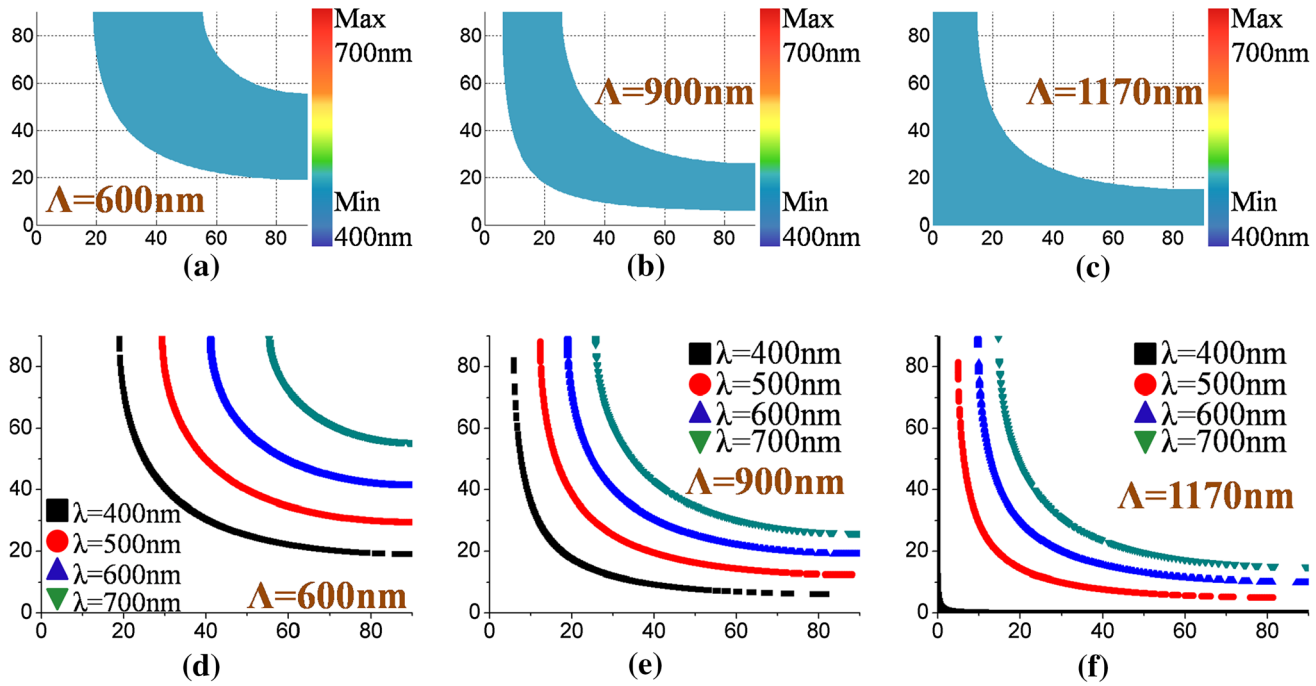

Fig. 5 Calculated coordinate and spectrum for the structural colors formed under the spatial periods of 400 and 500 nm

case, the four spectra lines appear together. In contrast, the spectra lines are located very close to each other, and they have the trend to get close to the origin of coordinates.

Secondly, the influence of spatial periods ranged from 522 to 1,170 nm on the diffracted spectrum is discussed, and the results are shown in Fig. 5. In this period scope, it is found that no matter what the location of the silhouette is, diffracted light can cover the whole spectrum (Fig. 5a–c). Similar to the previous, the locations of $\lambda = 400$, 500, 600 and 700 nm are getting closer to the

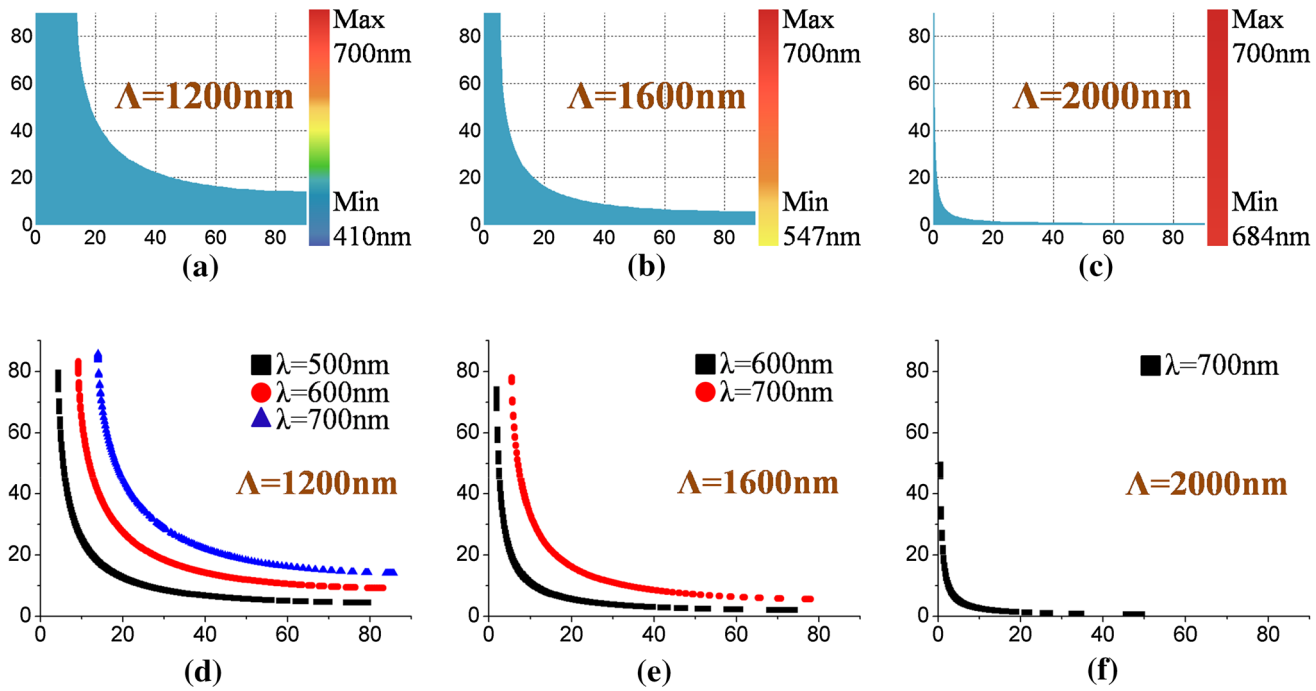

Fig. 6 Calculated coordinate and spectrum for the structural colors formed under the spatial periods ranged from 1,200 to 2,000 nm. The structural colors produced under spatial periods of 1,200, 1,300, 1,500 and 1,600 nm

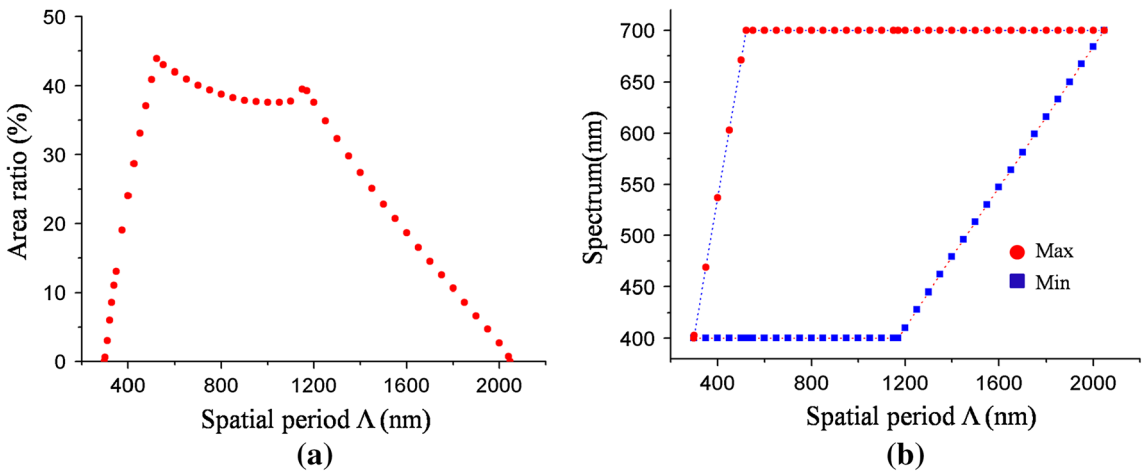

Fig. 7 **a** Ratio of silhouette area to total coordinate area. **b** Maximum value and the minimum value of the spectrum of the structural colors formed with different spatial periods

origin of coordinates, and the spectral lines are closer to each other (Figs. 5d–e).

In addition to the two period scopes discussed above, it is indicated that the spatial periods ranged from 1,170 to 2,047 nm also affect the diffracted spectrum greatly. The silhouette is becoming narrower with the increasing periods, leading to the diffracted light only covers a part of the visible spectrum, and the lower limit of the spectrum rises and the red shifts occur. The partial results are graphically expressed in Fig. 6.

As described above, the coordinate areas and the spectral ranges of the colors are affected by the spatial periods of the ripples. In order to demonstrate this effect, we have calculated the ratio of silhouette area to total coordinate area and the extremum of the spectrum formed under the whole spatial periods range. The results are illustrated in Fig. 7. From Fig. 7a, it is worth noticed that the ratio has two maximum values of 43.9 and 39.5 %, which are obtained at spatial periods of 522 and 1,170 nm, respectively. As for the spectrum range of the diffracted light, it

can be found from Fig. 7b that the spectrum range has a linear relation to the spatial periods of ripples.

Based on the above-mentioned discussion, it is not difficult to understand why the surfaces composed of ripples with different spatial periods exhibit very different colors. Furthermore, from Fig. 2, it is found that the colors are gradually changed from blue to red with the increase of periods under the same ripple orientation angle and incident light angle. At the approximate symmetric coordinate points, such as the points of (50°, 60°) and (70°, 50°) in Fig. 2a (20°, 85°) and (80°, 20°) in Fig. 2b, the colors are nearly identical. This can be attributed to the symmetry of the spectral lines about the angle bisector for coordinate. In Fig. 2c, it is obviously observed that the colors formed by the ripples with spatial period of 1,200 and 1,300 nm can cover most of the visible spectrum. While for the colors formed under spatial periods of 1,500 and 1,600 nm, only the spectrum longer wavelength can be covered. In addition, at many points, such as (10°, 40°), (10°, 50°), (10°, 90°) and so on, there is no wavelength of white light found to fulfill the diffraction conditions, thus no color can be observed. As for the ripples with spatial periods longer than 1,600 nm, the formed colors are not experimentally discussed, because the power of the laser at longer incident wavelength is reduced too rapidly to induce uniform ripples. However, the results give the experimental evidence that color effects depend on the ripple period strongly.

As described above, the theoretical and experimental analyses demonstrate that the colors are affected greatly by the ripples with different spatial periods. The study proposes the possibility of marking the metal surfaces with various colors which are formed by different laser wavelengths.

4 Conclusion

In summary, this paper has reported the study of various structural colors on stainless steel surface produced by femtosecond laser with different wavelengths, theoretically and experimentally. We find that ripples with various spatial periods can be induced by different wavelengths under suitable laser fluence and scanning speed. The ripples strongly affect the spectrum of the diffracted light. When a pattern is marked by ripples with various spatial periods, different vivid colors can be simultaneously observed under the same viewing conditions. This study offers a new controllable parameter to produce diverse colors, which may find a wide range of applications in the laser color marking, art designing and so on.

Acknowledgments This work was supported by National Science Foundation of China (No. 51275502, 11204250, 51405464 and 91223203), Anhui Provincial Natural Science Foundation (No.1408085ME104), National Basic Research Program of China (No. 2011CB302100).

References

1. M. Huang, F. Zhao, Y. Cheng, N. Xu, Z. Xu, Two-dimensional periodic structure induced by single-beam femtosecond laser pulses irradiating titanium. Opt. Express **17**(23), 20756–20761 (2009)
2. L. Qi, K. Nishii, Y. Namba, Regular subwavelength surface structures induced by femtosecond laser pulses on stainless steel. Opt. Lett. **34**(12), 1846–1848 (2009)
3. Y. Tang, J. Yang, B. Zhao, M. Wang, X. Zhu, Control of periodic ripples growth on metals by femtosecond laser ellipticity. Opt. Express **20**(23), 25826–25833 (2012)
4. J. Yao, C. Zhang, H. Liu, Q. Dai, L. Wu, S. Lan, A.V. Gopal, V.A. Trofimov, T.M. Lysak, High spatial frequency periodic structures induced on metal surface by femtosecond laser pulses. Opt. Express **20**(2), 157813 (2012)
5. R. Wagner, J. Gottmanna, A. Horna, E.W. Kreutz, Subwavelength ripple formation induced by tightly focused femtosecond laser radiation. Appl. Surf. Sci. **252**(4), 8576–8579 (2006)
6. J. Wang, C. Guo, Ultrafast dynamics of femtosecond laser-induced periodic surface pattern formation on metals. Appl. Phys. Lett. **87**(25), 251914 (2005)
7. A.Y. Vorobyev, C. Guo, Femtosecond laser-induced periodic surface structure formation on tungsten. J. Appl. Phys. **104**(6), 063523 (2008)
8. A.Y. Vorobyev, V.S. Makin, C. Guo, Periodic ordering of random surface nanostructures induced by femtosecond laser pulses on metals. J. Appl. Phys. **101**(3), 034903 (2007)
9. J. Wang, C. Guo, Formation of extraordinarily uniform periodic structures on metals induced by femtosecond laser pulses. J. Appl. Phys. **100**(2), 023511 (2006)
10. A.Y. Vorobyev, C. Guo, Colorizing metals with femtosecond laser pulses. Appl. Phys. Lett. **92**(4), 041914 (2008)
11. B. Dusser, Z. Sagan, H. Soder, N. Faure, J.P. Colombier, M. Jourlin, E. Audouard, Controlled nanostructrures formation by ultrafast laser pulses for color marking. Opt. Express **18**(3), 2913–2924 (2010)
12. M.S. Ahsan, F. Ahmed, Y.G. Kim, M.S. Lee, M.B.G. Jun, Colorizing stainless steel surface by femtosecond laser induced micro/nano-structures. Appl. Surf. Sci. **257**(17), 7771–7777 (2011)
13. A.A. Ionin, S.I. Kudryashov, S.V. Makarov, L.V. Seleznev, D.V. Sinitsyn, E.V. Golosov, O.A. Golosova, Y.R. Kolobov, A.E. Ligachev, Femtosecond laser color marking of metal and semiconductor surfaces. Appl. Phys. A **107**(2), 301–305 (2012)
14. J. Yao, C. Zhang, H. Liu, Q. Dai, L. Wu, S. Lan, A.V. Gopal, V.A. Trofimov, T.M. Lysak, Selective appearance of several laser-induced periodic surface structure patterns on a metal surface using structural colors produced by femtosecond laser pulses. Appl. Surf. Sci. **258**(19), 7625–7632 (2012)
15. G. Li, J. Li, L. Yang, X. Li, Y. Hu, J. Chu, W. Huang, Evolution of aluminum surface irradiated by femtosecond laser pulses with different pulse overlaps. Appl. Surf. Sci. **276**(1), 203–209 (2013)
16. A.Y. Vorobyev, C. Guo, Spectral and polarization responses of femtosecond laser-induced periodic surface structures on metals. J. Appl. Phys. **103**(4), 043513 (2008)
17. T. Jia, H. Chen, M. Huang, F. Zhao, J. Qiu, R. Li, Z. Xu, X. He, J. Zhang, H. Kuroda, Formation of nanogratings on the surface of a ZnSe crystal irradiated by femtosecond laser pulses. Phys. Rev. B **72**(12), 125429 (2005)

18. S. Sakabe, M. Hashida, S. Tokita, S. Namba, K. Okamuro, Mechanism for self-formation of periodic grating structures on a metal surface by a femtosecond laser pulse. Phys. Rev. B **79**(3), 033409 (2009)
19. K. Okamuro, M. Hashida, Y. Miyasaka, Y. Ikuta, S. Tokita, S. Sakabe, Laser fluence dependence of periodic grating structures formed on metal surfaces under femtosecond laser pulse irradiation. Phys. Rev. B **82**(16), 165417 (2010)
20. J.P. Colombier, F. Garrelie, N. Faure, S. Reynaud, M. Bounhalli, E. Audouard, R. Stoian, F. Pigeon, Effects of electron-phonon coupling and electron diffusion on ripples growth on ultrafast-laser-irradiated metals. J. Appl. Phys. **111**(2), 024902 (2012)
21. H. Lochbihler, Colored images generated by metallic sub-wavelength gratings. Opt. Express **17**(14), 12189–12196 (2009)
22. H. Lochbihler, Two-dimensional subwavelength gratings with different frontside/backside reflectance. Opt. Lett. **38**(7), 1028–1030 (2013)
23. H. Lochbihler, Reflective colored image based on metal-dielectric–metal-coated gratings. Opt. Lett. **38**(9), 1398–1400 (2013)
24. G. Li, J. Li, Y. Hu, C. Zhang, X. Li, J. Chu, W. Huang, Realization of diverse displays for multiple color patterns on metal surfaces. Appl. Surf. Sci. **316**, 451–455 (2014)